Revolutionizing solid tumor surgery with Fibroblast Activation Protein (FAP) targeted imaging probes for a fluorescence-guided surgery of pancreatic cancer

Ma, H.Y.; Muynck, L.D.A.N. de; Houvast, R.D.; Beekman, S.; Piet, A.; March, T.L.; ... ; Seimbille, Y.

Bioconjugate Chemistry

pubs.acs.org/bc

Article

Revolutionizing Solid Tumor Surgery with Fibroblast Activation Protein (FAP)-Targeted Imaging Probes for a Fluorescence-Guided Surgery of Pancreatic Cancer

Hanyue Ma,[⊥] Lysanne D. A. N. de Muynck,[⊥] Ruben D. Houvast, Savanne Beekman, Amber Piet, Taryn L. March, Lukas J. A. C. Hawinkels, J. Sven D. Mieog, Alexander L. Vahrmeijer, and Yann Seimbille*

Cite This: *Bioconjugate Chem.* 2025, 36, 2145−2157

Read Online

ACCESS | Metrics & More | Article Recommendations | Supporting Information

ABSTRACT: The development of fluorescent probes that target the tumor stroma to help surgeons detect and remove malignant lesions using near-infrared fluorescence (NIRF)-guided surgery is advancing rapidly. Such advancements show promise for a range of malignancies, expanding the eligibility of patients for surgical intervention and offering improved surgical outcomes. Fibroblast activation protein (FAP), expressed by cancer-associated fibroblasts (CAFs), is highly upregulated within the tumor stroma of nearly all solid tumors. It is a promising tumor target for NIRF-guided surgery, especially in solid tumors with dense tumor stroma, such as pancreatic cancer. In this study, we aimed to develop FAP-targeting fluorescent probes with enhanced pharmacokinetics for the NIRF-guided surgery of pancreatic cancer. Three novel FAP-targeted probes (eFAPs) based on a (4-quinolinoyl)-glycyl-2-cyanopyrrolidine (QCP) structure equipped with the NIRF dye IRDye800CW were designed and synthesized. All of the probes displayed excellent inhibition potency and selectivity to FAP. The probes consistently exhibited strong inhibition and specific uptake in FAP-expressing U87 glioblastoma cells. In in vivo optical imaging studies, eFAP-24 showed a tumor-to-background ratio (TBR) of 3.1 ± 0.6 at 24 h postinjection, enabling the clear delineation of tumors using the clinical Quest Spectrum NIRF imaging system. A strong fluorescence signal in the tumor and a negligible uptake in nontarget tissues were confirmed by biodistribution analyses. The successful development and validation of FAP-targeting fluorescent probes, especially eFAP-24, offers promising prospects for enhancing the visualization of FAP-rich stromal compartments improving surgical outcomes through NIRF-guided surgery, particularly in solid tumors with dense stroma such as pancreatic cancer.

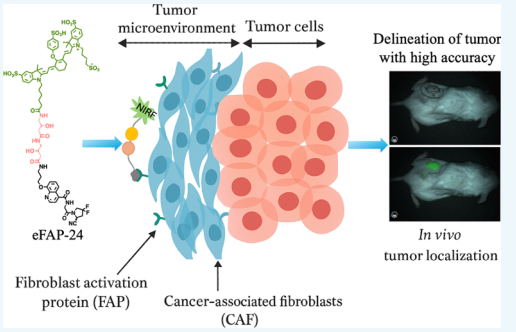

1. INTRODUCTION

Pancreatic cancer represents one of the most fatal malignancies, often diagnosed at a late stage due to its asymptomatic onset.[1] Surgical resection remains the only curative option, yet a majority of patients present with unresectable disease. Despite thorough preoperative imaging, such as CT scans, up to 80% of tumors are deemed inoperable during exploratory surgery, with occult metastases detected in up to 38% of cases. Achieving negative tumor margins (R0 resection) is crucial for reducing recurrence rates but remains a significant challenge.[2] Emerging technologies, including intraoperative near-infrared fluorescence (NIRF) imaging, offer the visualization of tumor-associated tissues in real-time, facilitating precise delineation of tumor margins and enhancing the likelihood of achieving complete R0 resections. NIRF imaging employs contrast agents that emit a fluorescence in the 700−900 nm range, which can be visualized by dedicated cameras and presented on a monitor. Targeted NIRF probes bind specifically to receptors expressed on tumors, with minimal binding to healthy tissues, enhancing precision during surgery. This technology holds promise in improving the completeness of resections and ultimately patient outcomes.[3]

The tumor microenvironment (TME) contains abundant cancer-associated fibroblasts (CAFs), which play a critical role in promoting tumor growth, progression, and metastasis.[4,5] One feature of CAFs is the expression of fibroblast activation protein (FAP), a type-II transmembrane glycoprotein that promotes tumor progression by supporting angiogenesis, remodeling the extracellular matrix, and immunosuppression. While the FAP expression is minimal in healthy tissues, it is significantly upregulated in pathological conditions, particularly in the CAFs

Received: May 13, 2025
Revised: September 4, 2025
Accepted: September 4, 2025
Published: October 1, 2025

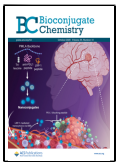

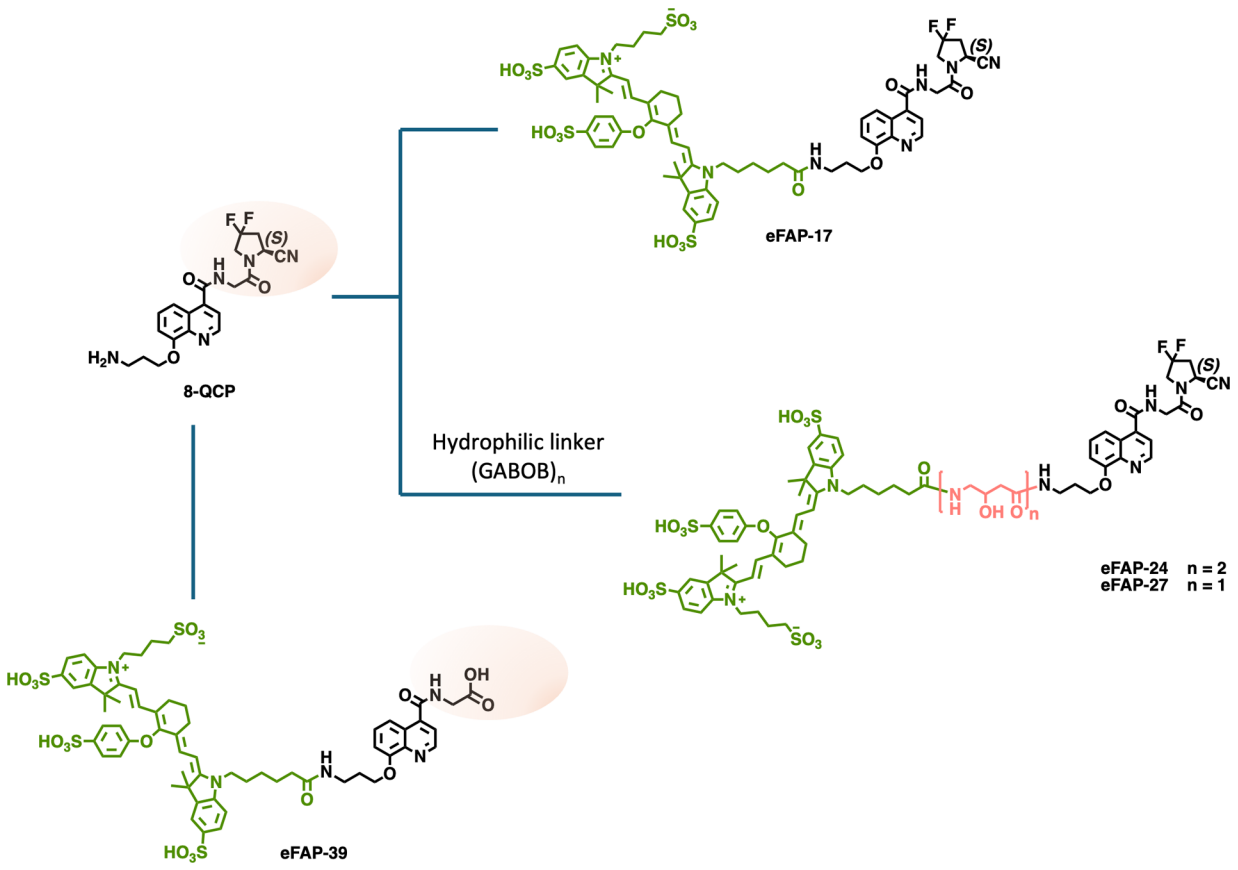

Figure 1. Chemical structure of IRDye 800CW (green) equipped FAP binding unit (8-QCP) with or without GABOB (red) linker (eFAP-17, eFAP-24, and eFAP-27) and the negative control eFAP-39. The difference between eFAP-17 and eFAP-39 is highlighted in orange.

of more than 90% of malignant epithelial tumors with dense stromal components,[6] such as pancreatic cancer.[7] In pancreatic cancer, where desmoplasia hinders effective drug delivery to tumor cells, targeting CAFs in addition to tumor cells offers a promising alternative because CAFs are abundant and more accessible within the stroma.[8,9] The development of tumor-targeting fluorescent probes to help surgeons detect and remove malignant lesions with a dense stroma using near-infrared fluorescence (NIRF)-guided surgery is advancing rapidly. Such advancements show promise for a range of malignancies and better visualization of metastases.

FAP inhibitors exhibiting a high binding affinity and specificity to FAP have been extensively studied. FAPI-04 and FAPI-46,[10,11] two of the most successful small-molecule-based inhibitors equipped with a metal chelator, have demonstrated a high in vivo tumor uptake, fast clearance from the circulation, and production of high-contrast PET/CT images in many types of cancer, such as sarcomas, cholangiocarcinoma, and cancers of the esophagus, breast, liver, lung, colon, head and neck, ovary, prostate, and pancreas.[12] [^{68}Ga]Ga-FAPI-04 PET/CT demonstrated a superior accuracy and sensitivity across primary lesions, distant metastases, and metastatic lymph nodes than [^{18}F]-FDG PET/CT in staging pancreatic cancer.[13] Dynamic imaging with [^{68}Ga]FAPI-04 and [^{68}Ga]FAPI-46 showed potential in distinguishing pancreatic cancer from pancreatitis, a challenging differentiation using static imaging alone.[14] These promising results have led to the consideration of FAP as a compelling molecular target for the NIRF-guided surgery of pancreatic cancer.

We recently developed a new highly potent FAP ligand, termed eFAP, which allows substitutions on the (4-quinolinoyl)-glycyl-2-cyanopyrrolidine (8-QCP) scaffold through the etherification at the 8-position of the quinoline ring. eFAP demonstrated a strong affinity to FAP at a low nanomolar range and has the capacity to be conjugated with various payloads, such as radionuclides, fluorophores, and cytotoxic drugs, for various applications in oncology. For example, in a mouse xenograft model, a DOTA chelator equipped eFAP-6 showed a high and rapid tumor uptake with a low background uptake in healthy organs.[15] The high-contrast imaging and rapid clearance, comparable to the clinical reference FAPI-46, suggested that our eFAP ligand is an ideal candidate for tumor-targeted imaging purposes. The encouraging results prompted us to develop new FAP-targeted fluorescent probes based on the eFAP scaffold for NIRF-guided surgery for pancreatic cancer using IRDye800CW as the NIR dye component. The efficacy of these new probes was subsequently investigated through various *in vitro* and *in vivo* studies.

2. RESULTS

2.1. FAP-Targeted NIRF Probes and Negative Control Design. eFAP-17, eFAP-24, and eFAP-27, three fluorescent probes comprised the 8-QCP backbone targeting FAP. All three probes were conjugated to the clinically validated NIRF dye, IRDye800CW. IRDye800CW was directly coupled to the 8-QCP scaffold for eFAP-17, while hydrophilic linkers based on 4-amino-3-hydroxybutanoic acid (GABOB) were introduced between the 8-QCP moiety and the dye to improve the hydrophilicity of eFAP-24 and eFAP-27. To facilitate a more

https://doi.org/10.1021/acs.bioconjchem.5c00218
Bioconjugate Chem. 2025, 36, 2145−2157

Scheme 1. Chemical Synthesis of the Boc-Protected 8-QCP (10) Core Structure[a]

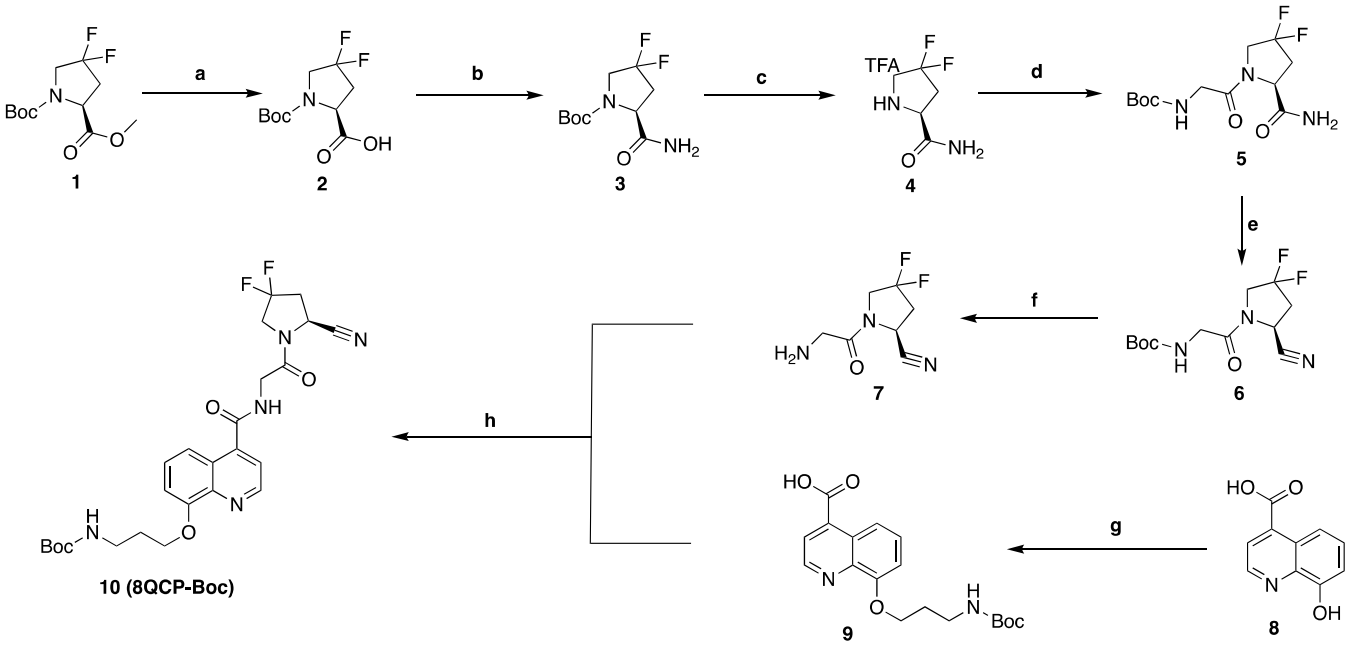

[a]Reagent and conditions: (a) NaOH, MeOH, 30 min, rt, 86%; (b) (i) *N*-hydroxysuccinimide, DCC, rt, 1 h (ii) NH_3 in MeOH, rt, 2 h, 72%; (c) TFA, DCM, 90%; (d) *N*-(*tert*-butoxycarbonyl)glycine, HBTU, DIPEA, rt, 2 h; (e) TFAA, pyridine, THF, −15 °C to rt, 3 h, 53%, over two steps; (f) TFA, DCM, quantitative; (g) (1) *tert*-butyl (2-bromoethyl)carbamate, Cs_2CO_3, DMF, rt, overnight; (2) NaOH, MeOH, rt, 30 min, 57%; (h) HBTU, DIPEA, DMF, rt, 2 h, 72%.

comprehensive evaluation of these eFAP probes in vivo, a negative control eFAP-39 was designed and synthesized. The structure of eFAP-39 closely resembles that of eFAP-17, except for the absence of the cyanopyrrolidine moiety, ensuring a similar metabolism and pharmacokinetics (see Figure 1).

2.2. Chemical Synthesis. The syntheses of (4-quinolinoyl)-glycyl-2-cyanopyrrolidine (8-QCP)-based FAP probes are presented in Schemes 1−3. Initially, 1-(*tert*-butyl)-2-methyl-(*S*)-4,4-difluoropyrrolidine-1,2-dicarboxylate was demethylated in a solution of NaOH in MeOH to achieve intermediate **2** in 86% yield. The amination of **2** was performed via activation into a NHS ester using *N*-hydroxysuccinimide and DCC in DMF, followed by treatment with an ammonia solution in MeOH, resulting in amide **3** in 72% yield. The *tert*-butyloxycarbonyl (Boc) protecting group on **3** was removed in a TFA/DCM mixture, affording compound **4** in a 90% yield. The deprotected **4**, containing a free secondary amine, was ready to be coupled with *N*-(*tert*-butoxycarbonyl)glycine in the presence of HBTU and DIPEA in DMF, affording intermediate **5**. The latter was then treated with trifluoroacetic anhydride and pyridine in THF to obtain the corresponding nitrile **6** in 53% yield over two steps. Etherification of 8-hydroxyquinoline-4-carboxylic acid (**8**) was conducted in a two-step procedure using *tert*-butyl (2-bromoethyl)carbamate in the presence of Cs_2CO_3, followed by treatment with NaOH in MeOH, providing **9** in a 57% yield over two steps. The removal of the Boc protecting group from **6** using TFA/DCM (1:1) prior to reacting it with quinoline **9** afforded the desired intermediate 8-QCP-Boc (**10**) in a yield of 72%.

To obtain the IRDye800CW-conjugated probe eFAP-17, the Boc-protecting group was removed from **10** using acidic conditions and the resulting amine **11** subsequently reacted with IRDye800CW-NHS ester, to give **12** (eFAP-17). Next, the core structure of 8-QCP was extended by the incorporation of GABOB units. This was achieved by reacting **11** with 4-((*tert*-butoxy carbonyl)amino)-3-hydrobutanoic acid. Repeated Boc deprotection and GABOB coupling led to the preparation of elongated compounds **13** and **15**, containing one and two GABOB units, respectively. Upon reacting with the IR-Dye800CW-NHS ester, fluorescent probes 14 (eFAP-27) and **16** (eFAP-24) were successfully synthesized.

2.3. Stability and Lipophilicity. Stability and hydrophilicity are important parameters when *in vivo* screening of compounds. Improved hydrophilicity, reflected by a lower Log *D* value, may contribute to enhanced solubility and reducing an off-targeted tissue uptake, which may also support higher probe stability in biological media.

The stability of eFAP-17, eFAP-24, and eFAP-27 was analyzed through LC analysis (Table 1, Figure S17) after incubation in Phosphate-Buffered Saline (PBS), mouse serum (MS), and human serum (HS) (n = 3). Both eFAP-24 and eFAP-27 showed a strong hydrophilic character with log $D_{7.4}$ values of −2.10 ± 0.31 and −1.62 ± 0.09, respectively. eFAP-17 demonstrated a more lipophilic nature (Log $D_{7.4}$ = −0.95 ± 0.02). The increased hydrophilic properties of eFAP-24 and eFAP-27 could be attributed to the introduction of GABOB linkers.

Additionally, all three eFAP probes exhibited outstanding stability in PBS for at least 24 h, showing less than 3% degradation. The highest stability was observed for eFAP-24, retaining 98.6 ± 1.44%, 97.7 ± 0.76%, and 98.5 ± 1.33% of its integrity in PBS, MS, and HS, respectively. eFAP-27 showed a decreased stability compared to eFAP-24 but remained >90% intact after 24 h. Although eFAP-17 was highly stable in PBS (97.5 ± 0.49%, at 24 h), a decrease in integrity was observed over time in MS and HS, resulting in 54.07 ± 5.52% and 82.22 ± 0.53% intact eFAP-17 at 24 h, respectively. The reduced stability of eFAP-17 compared to the other two probes is likely due to the

https://doi.org/10.1021/acs.bioconjchem.5c00218
Bioconjugate Chem. 2025, 36, 2145−2157

Scheme 2. Chemical Synthesis of the NIRF Probes eFAP-17, eFAP-24, and eFAP-27[a]

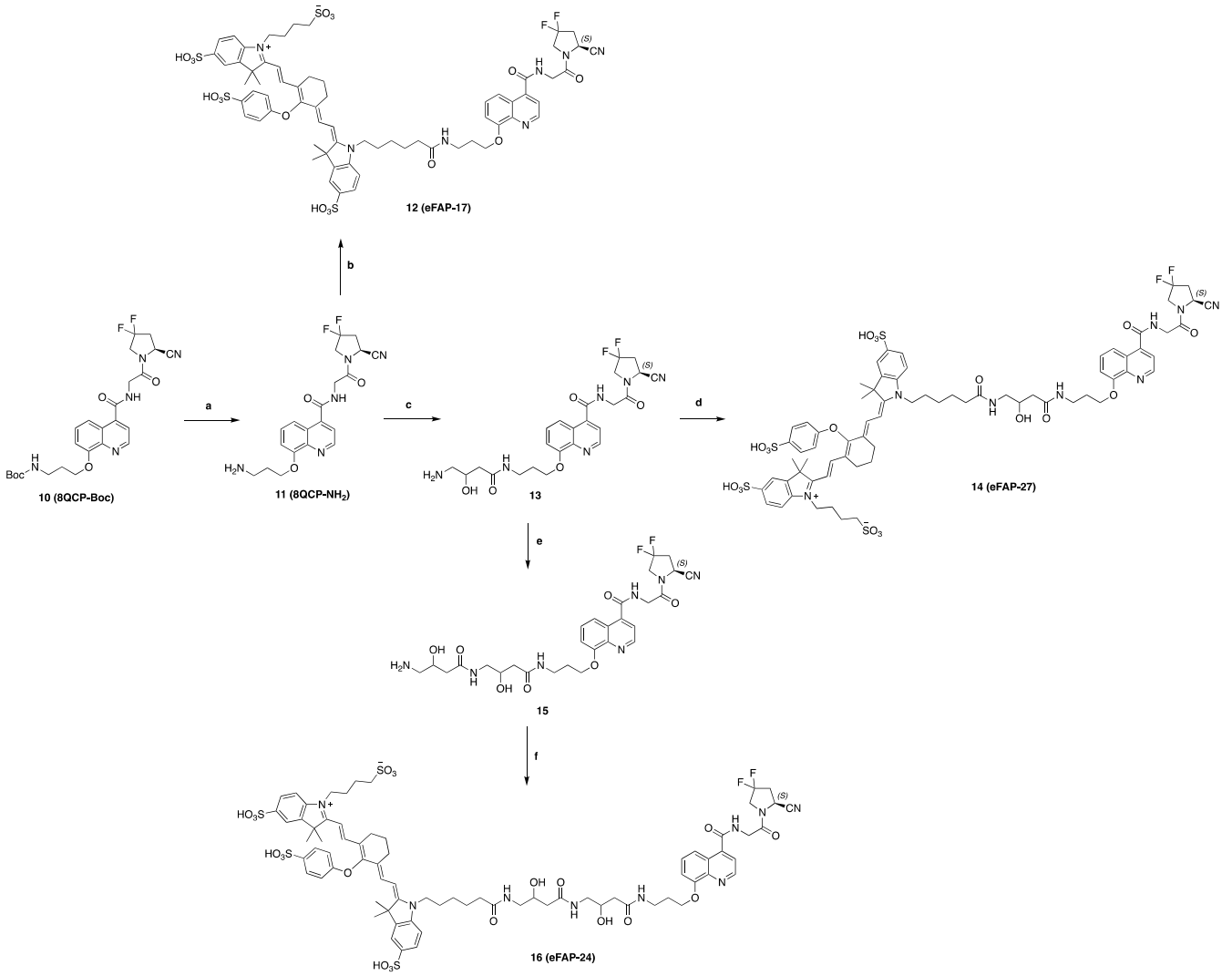

[a]Reagents and conditions: (a) TFA, TIPS, DCM, rt, 30 min; (b) 800CW-NHS, DIPEA, DMF, rt, dark conditions, 45 min, 85%; (c) (i) 4-((*tert*-butoxycarbonyl)amino)-3-hydrobutanoic acid, HBTU, DIPEA, DMF, rt, 1 h; (ii) TFA, TIPS, DCM, rt, 30 min, 80% over two steps; (d) 800CW-NHS, DIPEA, DMF, rt, dark conditions, 45 min, 79%; (e) (i) 4-((*tert*-butoxycarbonyl)amino)-3-hydrobutanoic acid, HBTU, DIPEA, DMF, rt, 1 h; (ii) TFA, TIPS, DCM, rt, 30 min, 41%, over two steps; (f) 800CW-NHS, DIPEA, DMF, rt, dark conditions, 45 min, 72%.To synthesize the negative control **19** (eFAP-39), quinoline **9** was reacted with methyl glycinate to yield **17** followed by the deprotection of the Boc and methyl protecting groups. The resulting amine **18** was coupled to IRDye800CW-NHS ester to give **19** (eFAP-39).

Scheme 3. Chemical Synthesis of the Negative Control eFAP-39[a]

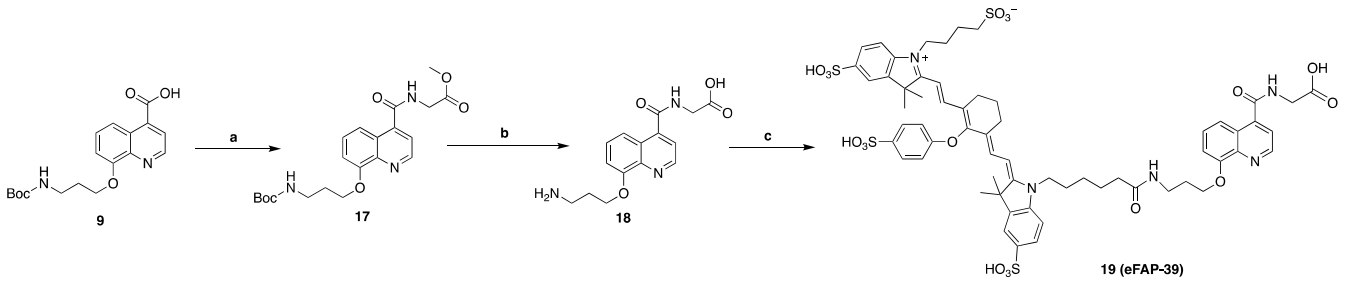

[a]Reagents and conditions: (a) methyl glycinate, HBTU, DIPEA, DMF, rt, 30 min; (b) (i) TFA, TIPS, DCM, rt, 30 min; (ii) NaOH, MeOH, 30 min, 30% over three steps; (c) 800CW-NHS, DIPEA, DMF, rt, dark conditions, 45 min, 69%.

lack of a linker between the dye and 8-QCP moiety, resulting in the direct coupling of the bulky IRDye800CW. This structural configuration may interfere with molecular stability, leading to greater degradation in the serum. Moreover, eFAP-39 showed no significant degradation when it was incubated for 24 h in PBS, MS, and HS.

https://doi.org/10.1021/acs.bioconjchem.5c00218
Bioconjugate Chem. 2025, 36, 2145−2157

Table 1. Lipophilicity (Log $D_{7.4}$) and Stability Studies

		stability (%, 24 h)		
	Log $D_{7.4}$	PBS	mouse serum	human serum
eFAP-17	−0.95 ± 0.02	97.5 ± 0.49	54.1 ± 5.52	82.2 ± 0.53
eFAP-24	−2.10 ± 0.31	98.6 ± 1.44	97.7 ± 0.76	98.5 ± 1.33
eFAP-27	−1.62 ± 0.09	97.8 ± 0.01	92.6 ± 2.23	96.6 ± 1.99
eFAP-39	−1.80 ± 0.19	97.6 ± 0.40	96.9 ± 1.39	99.0 ± 0.65

2.4. Binding Affinity. The inhibitory potency against human FAP (h.FAP) and murine FAP (m.FAP) proteins were determined in a recombinant enzymatic assay that relies on the cleavage of fluorescent AMC from a Z-Gly-Pro-AMC substrate. All three FAP probes exhibited a remarkable binding affinity to both h.FAP and m.FAP, with IC_{50} values in the low nanomolar range (IC_{50}, h.FAP < 6 nM, IC_{50}, m.FAP< 5 nM, Figures 2A and 3B, Table 2), comparable to FAPI-46 ($IC_{50,\ h.FAP}$ = 3.87 ± 2.7 nM, IC_{50},m.FAP = 1.55 ± 1.2 nM). Notably, eFAP-24 displayed the highest inhibitory activity against FAP (eFAP-24: IC_{50}, h.FAP = 3.04 ± 0.18 nM, IC_{50}, m.FAP = 2.96 ± 0.15 nM). Additionally, to evaluate the selectivity, enzymatic assays were conducted with prolyl oligopeptidase (PREP) and dipeptidyl peptidase IV (DPP4), proteins belonging to the same family as FAP. Similar to the FAP enzymatic assays, IC_{50} values for PREP and DPP4 were determined by incubating recombinant human PREP with a Z-Gly-Pro-AMC substrate and recombinant human DPP4 with H-Gly-Pro-AMC, respectively (Table 2, Figures 2C and 3D). All three probes demonstrated a micromolar affinity for PREP (IC_{50} = 0.32−2.00 μM), corresponding to high PREP/FAP selectivity indexes (SI) > 100. The IC_{50} values of eFAPs against DPP4 were in the low millimolar range, indicating a high selectivity in favor of FAP targeting (Table 2). The enzymatic assay of eFAP-39 on both h.FAP and m.FAP confirmed the extremely low binding of eFAP-39 to FAP proteins.

2.5. Cell Uptake. *In vitro* uptake studies were conducted on both FAP positive (U87) and FAP negative (U2OS) cell lines (Figure 3). Binding of all three probes to U87 was observed and exhibited concentration-dependent binding. Notably, binding of eFAP-17 and eFAP-27 reached saturation with 10 nM, while eFAP-24 still showed an increasing trend when treated with a higher concentration (Figure 3B). Consequently, among the probes, eFAP-24 demonstrated the highest accumulation (27.57 ± 2.02% AD), whereas eFAP-17 and eFAP-27 showed 3.55 ± 0.42% and 6.54 ± 0.81% AD, respectively (Figure 3D). A limited nonspecific binding of all probes was observed in FAP-negative U2OS cells when incubated with a high concentration (20 nM) of the probes (Figure 3A). Moreover, the negative control eFAP-39 did not show binding to both the FAP-positive and FAP-negative cell lines (Figure 3A−D).

2.6. *In Vivo* Binding Characteristics. With the highest binding affinity, stability, and superior uptake in FAP-positive cells, eFAP-24 was selected for further *in vivo* evaluation; eFAP-17 and eFAP-27 demonstrated a similar uptake, however, to assess the structural variations and the impact of hydrophilic linker introduction, eFAP-17 was chosen as the second probe *in vivo*, despite its slightly reduced stability. eFAP-39 served as a negative control.

The fluorescence intensity in the tumor was markedly higher than the background from 8 to 48 h post injection (p.i.) of eFAP-24 (Figure 4A). However, no such contrast could be visualized in mice administered with eFAP-17 and eFAP-39. The highest

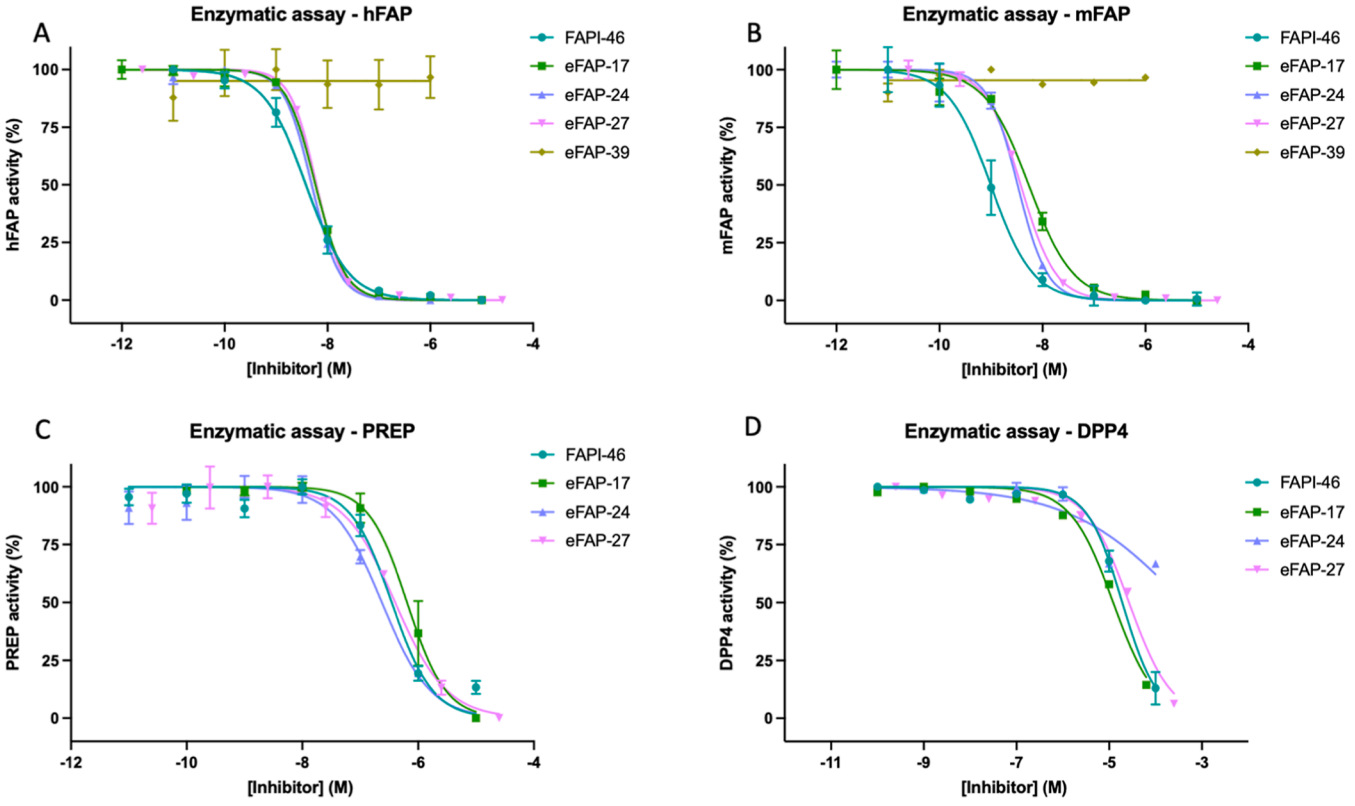

Figure 2. IC_{50} curves of FAPI-46, eFAP-17, eFAP-24, eFAP-27, and eFAP-39 on proteins. (A) Recombinant h.FAP. (B) Recombinant murine FAP. (C) Recombinant PREP. (D) Recombinant DPP4. All error bars represent standard deviations (SD).

https://doi.org/10.1021/acs.bioconjchem.5c00218
Bioconjugate Chem. 2025, 36, 2145−2157

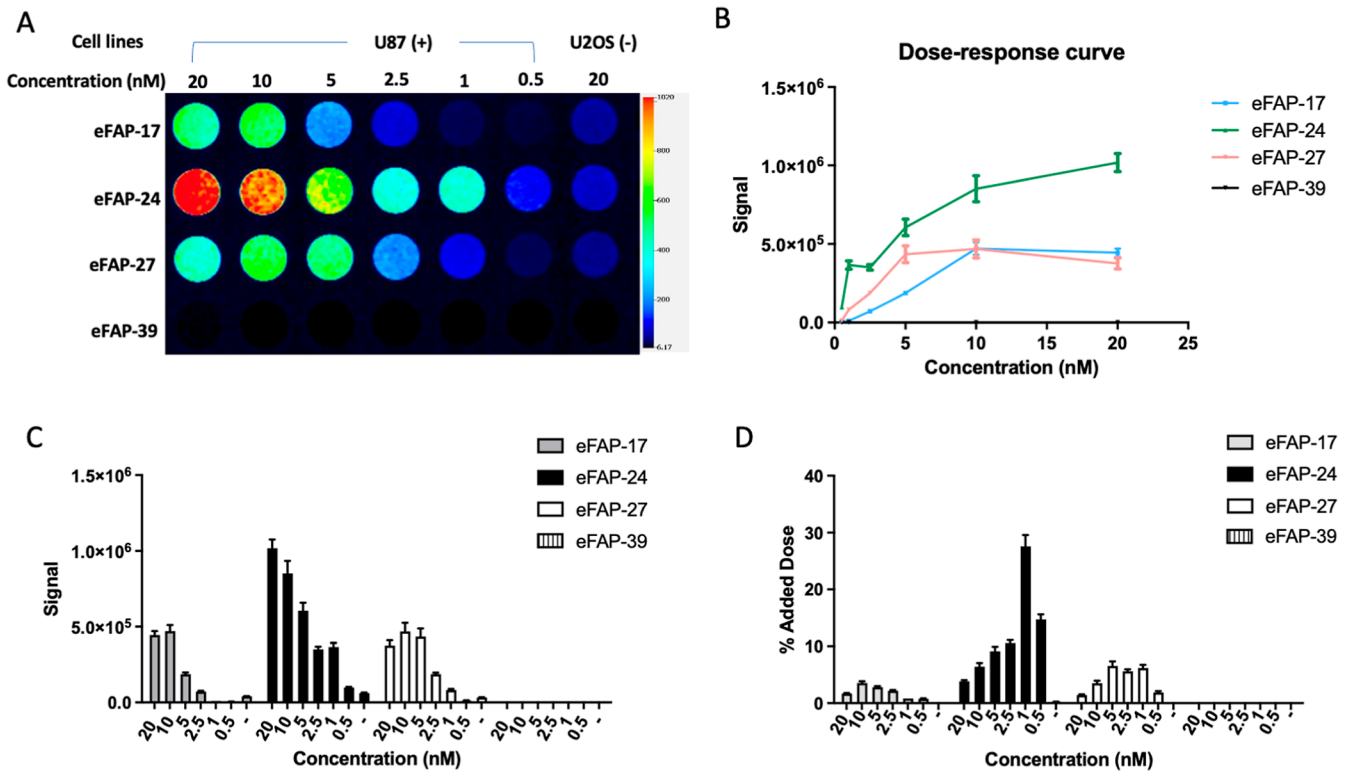

Figure 3. Cellular uptake studies on the FAP-positive cell line (U87) and FAP-negative cell line (U2OS). (A) Cells incubated with various concentrations of eFAPs were imaged to determine the binding of the eFAPs on U87 and U2OS cells. (B) Dose−response curves of eFAP probes and negative control binding to U87 cells. (C) Fluorescence signal of eFAPs (0.5−20 nM) binding to U87 and U2OS (displayed as (−) on the horizontal axis) cells. (D) Fluorescence signal of eFAPs (0.5−20 nM) binding to U87 and U2OS (−) cells normalized to the added dose. All error bars represent standard deviations (SD).

Table 2. IC_{50} Values Determined by an Enzymatic Assay and Selectivity Indexes[a]

	inhibition		selectivity		selectivity indexes (SI)	
	$IC_{50,h.FAP}$ (nM)	$IC_{50,m.FAP}$(nM)	$IC_{50,PREP}$ (nM)	$IC_{50,DPP4}$ (nM)	PREP/FAP	DPP4/FAP
FAPI-46	3.87 ± 2.7	1.55 ± 1.2	3480 ± 172.5	20,540 ± 2526	899.2	5307.5
eFAP-17	5.65 ± 0.19	5.0 ± 0.2	2000.7 ± 376.8	15,170 ± 4200	354	2685
eFAP-24	3.04 ± 0.18	2.96 ± 0.15	322.4 ± 43.8	13,587 ± 3970	106	4469
eFAP-27	4.01 ± 0.28	3.72 ± 0.11	667.3 ± 213.7	28,100 ± 2667	166	7007
eFAP-39	>1 mM	>1 mM	n.d.	n.d.		

[a]n.d.: not determined.

TBR (3.1 ± 0.6) was seen with eFAP-24 at 24 h p.i., allowing for clear tumor delineation using the clinical Quest Spectrum imaging system. A lower TBR was observed for eFAP-17 and the negative control eFAP-39 at 24 h p.i. (1.2 ± 0.1 and 0.9 ± 0.1, respectively) (Figure 4B,C). This emphasizes both the pharmacokinetic advantage and the improved binding affinity of the more hydrophilic and stable eFAP-24.

Biodistribution analyses at 48 h p.i. showed a high fluorescence signal in resected tumors of mice administered eFAP-24, accompanied by minimal fluorescence in healthy organs (Figure 5A,B). For eFAP-17 and eFAP-39, the fluorescence signal in the tumors was lower and was similar to the fluorescence signal in healthy organs. Although eFAP-24 showed a slightly increased fluorescence in excretory organs, including the kidneys and liver, compared to healthy tissue, higher tumor/kidneys (T/K) and tumor/liver (T/L) ratios were observed for eFAP-24 (T/K: 3.3, T/L: 5.3) compared to eFAP-17 (T/K: 1.8, T/L: 2.7) and eFAP-39 (T/K: 1.3, T/L: 1.8). An increased signal was also seen in the stomach for all three probes; however, this is a consequence of the presence of chlorophyll-containing alfalfa and its derivatives in mouse food, which is known to fluoresce in the NIR region. Using a clinically relevant stroma-rich organoid-based *in vivo* model of human PDAC, these findings highlight the superior potential of eFAP-24 as a tracer for FAP-targeted NIRF imaging of pancreatic cancer.

Histological analysis showed that eFAP-24 NIRF signals aligned with tumor stroma regions identified under the microscope and with FAP staining (Figure 5C), confirming probe specificity and complete tumor penetration.

3. DISCUSSION

NIRF-guided surgery holds great promise for improving radical resection rates by offering surgeons real-time visualization of the tumor tissue during operations. However, the ongoing difficult search for targeting molecules with optimal pharmacokinetics remains crucial, particularly in tumors with dense stroma such as pancreatic cancer. In this study, we developed three novel FAP-

https://doi.org/10.1021/acs.bioconjchem.5c00218
Bioconjugate Chem. 2025, 36, 2145−2157

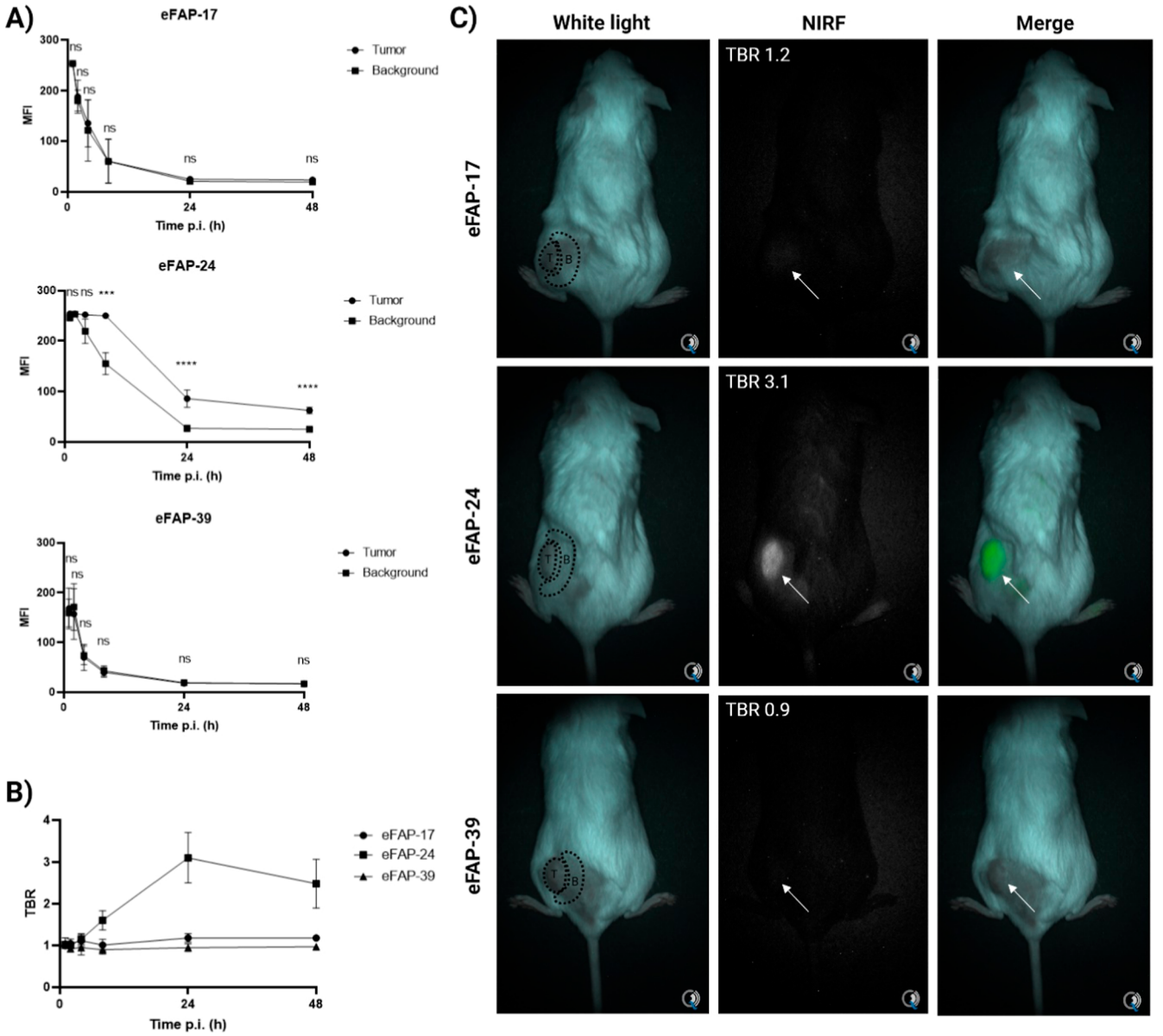

Figure 4. *In vivo* fluorescence imaging. (A) MFI's of eFAP-17, eFAP-24, and eFAP-39 of the tumor and corresponding background tissue. (B) TBR's of all three probes. (C) *In vivo* fluorescence images at 24 h. T; tumor, B; background. White arrows point at tumors. ns: not significant, ***p = 0.0001, ****p = < 0.0001.

targeted fluorescent probes—eFAP-17, eFAP-24, and eFAP-27—conjugated with IRDye800CW dye for NIRF imaging and assessed their effectiveness for real-time FAP-mediated imaging in pancreatic cancer. Of these, eFAP-24 demonstrated high stability, a significant *in vitro* uptake, and the ability to clearly distinguish tumor lesions from the surrounding tissue in a clinically relevant PDAC xenograft model, achieving the highest TBR *in vivo*. This study underscores the potential value of FAP-targeted imaging in addressing the unmet need for tools that improve tumor delineation during complex oncologic surgeries.

Targeting tumor cell surface receptors is a traditional approach for NIRF imaging due to their high specificity for cancer cells. However, the challenge arises from the heterogeneity of the receptor expression, which can vary between tumors and even within different areas of the same tumor, potentially resulting in incomplete visualization during surgery.[16] In contrast, targeting the tumor stroma offers several advantages, especially in cancers with a dense fibrotic tissue, like pancreatic cancer.[17] FAP is abundantly expressed in CAFs in the stromal compartment surrounding the tumor. Due to their high genetic stability and homogeneity, CAFs enable more consistent and widespread targeting across different tumors.[9,18] This approach ensures that even poorly vascularized, hypoxic, or necrotic tumor regions that are difficult to access with cell-targeting agents can still be targeted by NIRF probes. This makes it particularly advantageous for NIRF-guided surgery, especially in challenging surgical environments, such as pancreatic cancer, where the precision of visualization is even more critical as surgeons can no longer rely on tactile feedback for tumor identification. However, because the FAP expression reflects stromal remodeling rather than direct malignant cell activity, it may not correlate with tumor grade, aggressiveness, or viability. Combining tumor-cell-specific targets with FAP may offer a more comprehensive and accurate tumor visualization.

https://doi.org/10.1021/acs.bioconjchem.5c00218
Bioconjugate Chem. 2025, 36, 2145−2157

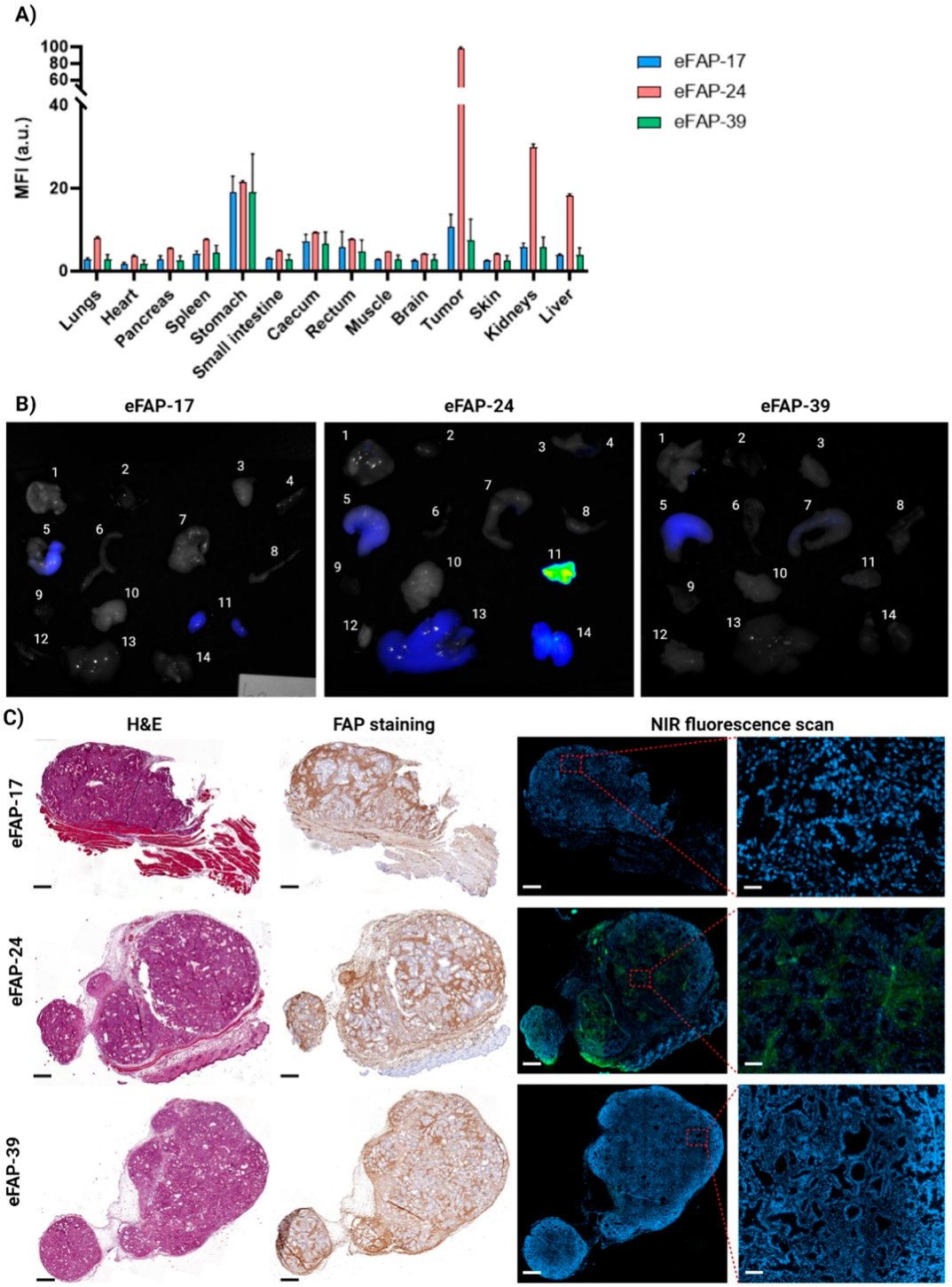

Figure 5. *Ex vivo* analysis of eFAP-17, eFAP-24, and eFAP-39. (A) MFIs of resected organs. (B) Fluorescence images of resected organs taken with the Pearl imaging system. (C) H&E, immunohistochemistry, and NIR fluorescence images of resected tumors. Scale bars represent 500 μm. Scale bars in zoomed in fluorescence images represent 50 μm. 1: lungs, 2: heart, 3: pancreas, 4: spleen, 5: stomach, 6: duodenum, 7: cecum, 8: rectum, 9: skin, 10: brain, 11: tumors, 12: skin, 13: liver, 14: kidneys.

Our novel probes featuring the (4-quinolinoyl)-glycyl-2-cyanopyrrolidine backbone as the FAP-binding moiety were synthesized via a rapid and straightforward procedure. All probes exhibited nanomolar inhibition of both h.FAP and m.FAP (IC_{50} < 6 nM), suggesting a limited influence of the modification at the 8-position of QCP on the binding affinity of the eFAP analogs. The introduction of the GABOB linkers enhanced the IC_{50} against FAP, confirming that an increased distance between the dye and QCP is required to preserve the binding affinity. The minor loss of affinity likely results from the bulk structure of the NIRF dye hindering the binding moiety from accessing the binding pocket on FAP. Additionally, similar to FAP, the inclusion of GABOB resulted in better inhibitory activity against PREP, which led to the less selectivity of the probes to FAP. Nevertheless, with high PREP/FAP and DPP4/FAP selectivity indexes (SI: PREP/FAP > 100, SI: DPP4/FAP >

https://doi.org/10.1021/acs.bioconjchem.5c00218
Bioconjugate Chem. 2025, 36, 2145−2157

2000), the eFAP probes retained high specificity. The hydrophilic character of GABOB also contributed to improved hydrophilic properties of the fluorescent probes. Moreover, all probes remained highly stable in PBS, MS, and HS for up to 4 h, showing <5% degradation. Among the probes, eFAP-24, which possesses two GABOB units, exhibited the highest inhibitory activity against h.FAP and m.FAP (3.04 ± 0.18 and 2.96 ± 0.15 nM, respectively) and the highest hydrophilicity (Log $D_{7.4}$ = −2.10 ± 0.31). Notably, eFAP-24 exhibited the greatest stability, maintaining over 97% integrity in PBS, MS, and HS after 24 h.

eFAP-24 also stood out among the synthesized probes, with its favorable *in vivo* performance. Its ability to clearly delineate tumor lesions from the surrounding healthy tissue with a high TBR of 3.1 in a clinically relevant tumor model is particularly noteworthy. This is especially important for pancreatic cancer, where distinguishing tumors from healthy pancreatic tissues is critical to achieve complete resection while preserving as much healthy tissue as possible. A TBR of 3.1 is promising and is in line with results from previous *in vivo* studies.[19−23] Moreover, by incorporating IRDye800CW, a dye already proven safe in clinical studies,[24−26] we enhance the translational potential of eFAP-24 for clinical use. The use of a targeting molecule with a relatively lower weight will facilitate an easier, more cost-effective, and straightforward synthesis, thereby further enhancing the potential for clinical translation. The use of a clinically relevant NIR camera system further strengthens the case for its integration into surgical workflows, enabling real-time imaging of FAP-expressing tumors and potentially improving patient outcomes by guiding more accurate tumor resection. Additionally, by focusing on FAP, a hallmark of desmoplasia, the probe could not only allow for tumor-specific imaging but also provide insights into the stromal contribution to tumor biology. This dual functionality could have applications beyond surgery, such as in monitoring therapy response or imaging fibrotic/stenotic lesions in the colon in patients with inflammatory bowel disease.

A limitation of this study is that FAP expression in tumor tissues after neoadjuvant therapy was not comprehensively evaluated. Although a previous study from our group investigated the expression of FAP, among other markers, in the PDAC tissue after neoadjuvant therapy, it was based on a small cohort and utilized a different antibody.[27] It is important to note that FAP antibodies have demonstrated a considerable variation in their effectiveness. Neoadjuvant therapy is increasingly employed to enhance survival and R0 resection rates in pancreatic cancer but can significantly reduce target expressions.[28,29] If the FAP expression is diminished post-therapy, the utility of eFAP probes for intraoperative imaging might be compromised, as tumors may not be sufficiently visualized during surgery. However, therapies usually target rapidly dividing cells, which is not the case for fibroblasts. Additionally, fibroblasts are known to be more resistant to conventional therapies.[4] Moreover, inflammation and fibrosis/necrosis caused by radio- and chemotherapy can lead to an increased FAP expression in the surrounding tissue, leading to elevated background signals. This heightened background signal complicates the ability to distinguish tumor boundaries from the background tissue during surgery. Unfortunately, the current literature on the FAP expression post-NAT is limited, and the data is conflicting. These underscore the importance of future studies to investigate how the FAP expression changes in response to neoadjuvant therapy.

Additionally, while eFAP-24 showed favorable *in vitro* and *in vivo* binding characteristics, the highest TBR was observed after 24 h despite an increase in mean fluorescence intensity (MFI) over time. This is attributed to the presence of the GABOB linker, which prolongs the tumor retention of the probe. Ideally, we would like to inject a probe just before surgery to avoid requiring the patient to visit the hospital multiple times. However, in this case, it may still be worthwhile to have the patient come in a day earlier, as long as the probe provides a significant benefit for the patient during surgery. A complementary biodistribution study at early time points is necessary to gain insight into the pharmacokinetics of eFAP-24 and better understand the influence of the linker.

Our findings establish eFAP-24 as a groundbreaking candidate for NIRF-guided surgery in pancreatic cancer, demonstrating enhanced tumor specificity, optimized pharmacokinetics, and real-time imaging capabilities that surpass existing probes. This study not only addresses a critical need in pancreatic cancer surgery but also sets a new standard for targeting stromal biomarkers, potentially transforming imaging strategies for various FAP-expressing tumors. The ability of eFAP-24 to enhance the intraoperative visualization of tumor margins is particularly relevant in reducing the incidence of positive resection margins, a key determinant of patient prognosis. Future research will aim to refine eFAP-24 for clinical applications, further building its significant potential for improving surgical outcomes and patient management in oncology.

4. MATERIALS AND METHODS

4.1. General Methods. Detailed information on general methods of chemistry and biology is provided in the Supporting Information.

4.2. Synthesis of 8-QCP-Boc Core Intermediate. 8-QCP-Boc was synthesized through a multistep organic synthesis procedure (Scheme 1). Detailed information on synthesis methods, HPLC, MS, and NMR characterizations of intermediates (**2**−**11**, **13**, **15**, and **17**−**18**) is provided in the Supporting Information (Supporting Information, Figures S1−S16).

4.3. Synthesis of IRDye800CW Equipped Probes: eFAP-17, eFAP-24, and eFAP-27 (Scheme 2). Probes were synthesized by coupling the corresponding amines (**11**, **13**, or **15**) with IRDye800CW-NHS and DIPEA in DMF at room temperature for 45 min in the dark. For eFAP-17, amine **11** (1.6 mg, 3.90 mmol) was reacted with IRDye800CW-NHS (5.0 mg, 4.29 mmol) and DIPEA (4.3 μL, 21.45 mmol). After concentration and purification by a Sep-Pak C18 cartridge, eFAP-17 was obtained (4.7 mg, 85% yield, 97% purity; ESI-MS m/z 1403.00 [M + H]+). Similarly, eFAP-27 was synthesized from compound **13** (2.0 mg, 79% yield, 98% purity; ESI-MS m/z 1504.40 [M + H]+), and eFAP-24 from compound **15** (2.4 mg, 72% yield, 96% purity; ESI-MS m/z 1605.40 [M + H]+). Detailed NMR spectra and analytical data are provided in the Supporting Information.

4.4. Synthesis of the Negative Control: (eFAP-39, Scheme 3): Similar to other probes, eFAP-39 was obtained from **18** (1.2 mg, 3.90 mmol) as a dark green powder (3.4 mg, 69% yield, 95% purity; ESI-MS m/z 1289.30 [M + H]+; HPLC Rt = 3.638 min). Detailed NMR spectra and analytical data are provided in the Supporting Information.

4.5. Stability in Phosphate-Buffered Saline (PBS), Mouse Serum, and Human Serum. Stability studies of

https://doi.org/10.1021/acs.bioconjchem.5c00218
Bioconjugate Chem. 2025, 36, 2145−2157

800CW-eFAPs and eFAP-39 were performed by incubation of the compound (50 μL, 1×10^{-4} M) in PBS (450 μL) at 37 °C for up to 24 h. Aliquots from the PBS solution were directly analyzed by LC−MS at 1, 4, and 24 h postincubation. Similarly, 50 μL of each compound (10^{-4} M) was incubated at 37 °C with 450 μL of mouse or human serum for up to 24 h. At 1, 4, and 24 h, 50 μL of the serum incubation mixture was combined with acetonitrile (50 μL) in an Eppendorf tube, followed by centrifugation (5000*g*) for 20 min. The resulting supernatant was then analyzed by LC−MS.

4.6. Determination of Log $D_{7.4}$ Values. The distribution coefficients (Log $D_{7.4}$) were measured by using the shake-flask method. Briefly, 30 μL of each 800CW-eFAPs solution (10^{-3} M) was mixed with 1 mL of PBS (0.01 M, pH 7.4) and *n*-octanol (*v*/*v*, 1:1) in an Eppendorf tube. Following vigorous vortexing, the mixture was centrifuged for 15 min at 2500*g* to separate the phase. Aliquots (3×50 μL) from both the aqueous and octanol phases were collected and analyzed via LC−MS. Log $D_{7.4}$ was calculated as Log $D_{7.4}$ = log[(area in octanol phase)/(area in aqueous phase)] and the experiment was performed in triplicate.

4.7. *In Vitro* Inhibition Studies. Enzymatic assays were performed on black 384-well plates, measuring fluorescence (E_x/E_m: 355/485 nm) on a microplate reader. For h.FAP and m.FAP, the reaction mixture comprised Z-Gly-Pro-AMC (10 μM), protein (10 ng), assay buffer (50 mM Tris, 100 mM NaCl, 1.5 μM BSA, pH 7.4), and serially diluted probes (10^{-5}−10^{-11} M, 1% DMSO) in 50 μL. Val-boroPro (10^{-4} M) and assay buffer (1% DMSO, v/v) served as positive and negative controls. Samples were incubated in the dark for 1 h at 37 °C. The PREP assay contained Z-Gly-Pro-AMC (1 μM), PREP (10 ng), and the same assay buffer as FAP, with probes diluted 10^{-4}−10^{-10} M. The DPP4 assay used H-Gly-Pro-AMC (100 μM) and DPP4 (0.5 nM) in an assay buffer of 50 mM Tris, 100 mM NaCl, pH 8, with probes diluted 10^{-4}−10^{-10} M. Plates were incubated at 37 °C for 15 min (PREP) or 30 min (DPP4). Val-boroPro and sitagliptin were used as positive controls. All assays were conducted in triplicate and repeated thrice.

4.8. Cell Lines and Culture for *In Vitro* Uptake Experiments. U87 cells and U2OS cells were used for the cell-based fluorescent uptake experiment as FAP-positive and FAP-negative cells, respectively. Cells were cultured in Dulbecco's Modified Eagle Medium (Gibco, Paisley, UK) supplemented with 2 mM L-glutamine, 10% fetal bovine serum (FBS), 50 U/mL penicillin, and 50 μg/mL streptomycin (Sigma-Aldrich, Amsterdam, The Netherlands). Cell lines were passaged twice weekly in tissue culture flasks using trypsin/ethylenediaminetetraacetic acid (trypsin/EDTA) (0.05%/0.02% w/v) and cultured at 37 °C in a humidified chamber with 5% CO_2.

Cell line selection rationale: for the *in vitro* evaluation of probe specificity and uptake, U87 glioblastoma cells were used. These cells are widely used as a model for FAP-targeted tracer development due to their robust and homogeneous expression of human FAP, enabling the reproducible quantification of FAP-specific binding and uptake. To address relevance to pancreatic cancer, *in vivo* imaging was performed using a clinically relevant PDAC coculture xenograft model (see Section 4.10.1).

4.9. Cell Uptake Experiments. For *in vitro* uptake studies, compounds were prepared in a 5% DMSO solution to prevent stickiness. U87 cells were detached with 0.05% trypsin (Corning; Amsterdam, The Netherlands) and resuspended (1×10^6 cells/tube) in binding buffer (PBS, 0.5% FBS, 2 mM EDTA), followed by incubation with compounds at 0−20 nM for 1 h at 37 °C in 5% CO_2. FAP-negative U2OS cells were treated similarly with 20 nM compound as a negative control. To assess nonspecific dye binding, cells were incubated with IRDye800CW (0−20 nM) alone. After incubation, cells were washed three times with ice-cold PBS (1 mL, 5% DMSO), resuspended in binding buffer, and plated (2×10^5 cells/well) in 96-well plates. NIR-fluorescence imaging was performed on an Odyssey scanner (800 nm channel), and images were collected with Empiria Studio, correcting the fluorescence intensity for the background signal.[30]

4.10. *In Vivo* Imaging. *4.10.1. Patient-Derived Organoids for In Vivo Use.* Organoid cultures were established from the human pancreatic cancer tissue obtained during surgical resection in accordance with the Code of Conduct for Responsible Use of Human Tissues after written informed consent was obtained from the patients. Organoid cultures were established and cultured as previously described.[31] This study was approved by the medical ethics Committee of the Leiden University Medical Center (RP24.004). hPS1 cells were a kind gift of Dr. Regan Koch (Queen Mary Hospital, London, UK).

4.10.2. In Vivo Fluorescence Imaging. Six- to 12 week-old female NSG (NOD.Cg-Prkdc^{scid} Il2rg^{tm1Wjl}/SzJ) mice were bred in-house and kept at the Central Animal Facility at LUMC and housed per EU Recommendation of 2007−526 EC under specific pathogen-free conditions. Mice were subcutaneously injected with a combination of 250,000 organoid cells (1 well), mixed with 2×10^6 hPS1 cells (1:8 ratio, reflecting CAF/tumor cell ratios in human PDAC) in a Matrigel into the left flank. Tumor growth was monitored with a digital caliper.

Mice bearing subcutaneous tumors of 50 mm^3 were administered with 2 nmol of either eFAP-17, eFAP-24, or eFAP-39 in 100 μL of PBS containing Kolliphor (60 μg/mL) and 2% DMSO via tail vein injection (n = 5 per group). Prior to imaging, the tumor and directly adjacent skin were shaved. Fluorescence imaging was performed using the clinical Quest Spectrum imaging system (Quest Medical Imaging; Wieringerwerf, The Netherlands) at 1, 2, 4, 8, and 24 h postinjection (p.i.), with animals maintained under 2−4% isoflurane anesthesia. After the final time point, animals were sacrificed, and the tumors along with major organs were resected for *ex vivo* imaging on the Pearl Trilogy Small Animal imaging system (LI-COR Biosciences; Lincoln, Nebraska USA) to evaluate the biodistribution based on fluorescence signals. Regions of interest (ROIs) were drawn around the tumor and the adjacent background, and tumor-to-background ratios (TBRs) were calculated by tumor mean fluorescence intensity (MFI)/background mean signal. For biodistribution analyses, MFIs were determined by drawing ROIs around the organs. Data from Quest images were processed with Spectrum Capture Suite (Quest Medical Imaging) and ImageJ (version 1.50, National Institutes of Health, Bethesda, MD, USA), while Pearl images were quantified using Image Studio (version 5.2, LI-COR).

4.10.3. Histological Analysis. Resected tumors were fixed in 4% paraformaldehyde for 24 h, replaced by ethanol, and subsequently embedded in paraffin. Formalin-fixed paraffin-embedded (FFPE) tissue blocks were sectioned at 4 μm thickness. For FAP immunohistochemistry, slides were first dehydrated in xylene and rehydrated through graded alcohol series. This was followed by incubation with 0.3% hydrogen peroxide for 20 min to block endogenous peroxidase activity. Heat-induced antigen retrieval was carried out in Tris/EDTA buffer (pH 9.0, Dako, Glostrup, Denmark) at 95 °C using a PT-Link module (Agilent; Santa Clara, CA, USA). Afterward, slides

https://doi.org/10.1021/acs.bioconjchem.5c00218
Bioconjugate Chem. 2025, 36, 2145−2157

were placed overnight in a humidified chamber at rt with a rabbit antihuman FAP monoclonal antibody (1/300, Abcam AB207178). Following three PBS washes, sections were incubated with a horseradish peroxidase (HRP)-labeled antirabbit secondary antibody (Envision, Dako) at rt for 30 min. Following PBS washes, the immunoreaction was developed with DAB substrate buffer (Dako) for 10 min and subsequently counterstained with Mayer's hematoxylin for 15 s. Slides were then dehydrated at 37 °C and mounted with Pertex (Leica Microsystems; Wetzlar, Germany). For histological reference, hematoxylin and eosin (H&E) staining was also performed on each FFPE block. All stained slides were digitalized with a Panoramic Digital Slide Scanner and viewed with CaseViewer 2.6 (3D Histech; Hungary). For fluorescence imaging, sections were deparaffinized in xylene, left to evaporate for 1−2 h, and cover slipped with a EverBrite Hardset Mounting Medium with DAPI (Biotium; Fremont, CA, USA) followed by fluorescence imaging using the ZEISS Axio Scan.Z1 (Carl Zeiss) and the acquired data were processed using Zen Lite (version 3.9, Carl Zeiss).

4.11. Statistics. Data were expressed as the mean ± standard deviation (SD). Statistical analyses were carried out using GraphPad Prism version 9.0 (San Diego, California USA). IC_{50} values were calculated by nonlinear regression Log(inhibitor) vs response analysis with a variable slope (four-parameters). All *in vitro* experiments were performed in triplicate and repeated three times. For *in vivo* experiments, $n = 5$ mice per group/time point were imaged, as at least three are needed to calculate the standard deviation, with two extra included to account for a potential dropout or the lack of tumor growth. MFI's were calculated from all five mice per time point, with each measurement taken from distinct mice (no repeated measurements). A two-way ANOVA (two-sided) was used to assess differences in the MFI across time points. Sidak's multiple comparison tests for the adjustment of multiple comparison was applied. Camera settings (exposure time of 100 ms) were kept constant for all measurements to ensure consistency. Figures were created with BioRender.com (full license).

■ ASSOCIATED CONTENT

Data Availability Statement

All data are available in the main text or the Supporting Information.

Supporting Information

The Supporting Information is available free of charge at https://pubs.acs.org/doi/10.1021/acs.bioconjchem.5c00218.

Experimental details, materials, and methods for the chemical synthesis of 8-QCP and its precursors, as well as general biological methods, 1H and 13C NMR spectra for intermediates and final probes, and LC−MS characterization of eFAP-17, eFAP-24, eFAP-27, and eFAP-39 (PDF)

■ AUTHOR INFORMATION

Corresponding Author

Yann Seimbille − *Departments of Radiology & Nuclear Medicine, Erasmus Medical Center, Rotterdam 3015 GD, The Netherlands; Erasmus Medical Center Cancer Institute, Rotterdam 3015 CP, The Netherlands;* orcid.org/0000-0002-9736-5318; Phone: +31 (0) 10 70 38961; Email: y.seimbille@erasmusmc.nl; Fax: +31 (0) 10 70 34033

Authors

Hanyue Ma − *Erasmus Medical Center Cancer Institute, Rotterdam 3015 CP, The Netherlands; Departments of Radiology & Nuclear Medicine, Erasmus Medical Center, Rotterdam 3015 GD, The Netherlands;* orcid.org/0009-0009-7307-0388

Lysanne D. A. N. de Muynck − *Department of Surgery, Leiden University Medical Center, Leiden 2333 ZA, The Netherlands*

Ruben D. Houvast − *Department of Surgery, Leiden University Medical Center, Leiden 2333 ZA, The Netherlands*

Savanne Beekman − *Departments of Radiology & Nuclear Medicine, Erasmus Medical Center, Rotterdam 3015 GD, The Netherlands; Erasmus Medical Center Cancer Institute, Rotterdam 3015 CP, The Netherlands*

Amber Piet − *Departments of Radiology & Nuclear Medicine, Erasmus Medical Center, Rotterdam 3015 GD, The Netherlands; Erasmus Medical Center Cancer Institute, Rotterdam 3015 CP, The Netherlands*

Taryn L. March − *Department of Surgery, Leiden University Medical Center, Leiden 2333 ZA, The Netherlands*

Lukas J. A. C. Hawinkels − *Department of Gastroenterology and Hepatology, Leiden University Medical Center, Leiden 2333 ZA, The Netherlands*

J. Sven D. Mieog − *Department of Surgery, Leiden University Medical Center, Leiden 2333 ZA, The Netherlands*

Alexander L. Vahrmeijer − *Department of Surgery, Leiden University Medical Center, Leiden 2333 ZA, The Netherlands*

Complete contact information is available at: https://pubs.acs.org/10.1021/acs.bioconjchem.5c00218

Author Contributions

[⊥]H.M. and L.D. contributed equally to this work. We acknowledge the contributions of all authors, with H. Ma and L. D. A. N. de Muynck contributing equally to this work. H. Ma performed the chemical synthesis, conducted in vitro experiments, acquired and analyzed the data, and contributed to manuscript preparation. L. D. A. N. de Muynck carried out the *in vivo* experiments, performed data acquisition, analysis, and interpretation, and contributed to manuscript preparation. R. D. Houvast contributed to *in vivo* experiments, data acquisition, analysis, and interpretation. S. Beekman and A. Piet conducted in vitro experiments and contributed to data acquisition, analysis, and interpretation. T. L. March synthesized the NIRF dye. L. J. A. C. Hawinkels contributed to the study design and provided the *in vivo* model. J. S. D. Mieog and A. L. Vahrmeijer conceptualized the study, designed the experiments, and supervised the project, with the contribution to a manuscript review. Y. Seimbille supervised the project, provided a critical input throughout the study, and contributed to a manuscript review. All authors contributed to the discussion of the manuscript content and reviewed and edited the manuscript before submission.

Notes

This research was conducted in compliance with medical ethics Committee of Leiden University Medical Center (RP24.004), and no ethical concerns were identified. The local animal welfare body of the LUMC reviewed and approved all animal studies. Animals were humanely cared for in accordance with the Code of Practice Animal Experiments in Cancer Research and guidelines from Directive 2010/63/EU of the European Parliament on the protection of animals used for scientific

https://doi.org/10.1021/acs.bioconjchem.5c00218
Bioconjugate Chem. 2025, 36, 2145−2157

purposes. Local standard operating procedures were followed for handling of animals.
The authors declare no competing financial interest.

■ ACKNOWLEDGMENTS

The authors gratefully acknowledge P. Kinderman, S. Hakuno, and N. Dam from the Department of Gastroenterology and Hepatology at the Leiden University Medical Center for a technical support and financial support from the EMC research innovation program, Erasmus Medical Center.

■ ABBREVIATIONS

CAF, cancer-associated fibroblast
FAP, fibroblast activation protein
FAPI, fibroblast activation protein inhibitor
QCP, (4-quinolinoyl)-glycyl-2-cyanopyrrolidine
FGS, fluorescence guided surgery
NIRF, near-infrared fluorescence
PREP, prolyl endopeptidase
DPP4, dipeptidyl peptidase-4
h.FAP, human fibroblast activation protein
m.FAP, murine fibroblast activation protein

■ REFERENCES

(1) Bengtsson, A.; Andersson, R.; Ansari, D. The actual 5-year survivors of pancreatic ductal adenocarcinoma based on real-world data. *Sci. Rep.* **2020**, *10*, 16425.
(2) Ethun, C. G.; Kooby, D. A. The importance of surgical margins in pancreatic cancer. *J. Surg. Oncol.* **2016**, *113*, 283−288.
(3) Mieog, J. S. D.; Achterberg, F. B.; Zlitni, A.; Hutteman, M.; Burggraaf, J.; Swijnenburg, R. J.; Gioux, S.; Vahrmeijer, A. L. Fundamentals and developments in fluorescence-guided cancer surgery. *Nat. Rev. Clin. Oncol.* **2022**, *19*, 9−22.
(4) De, P.; Aske, J.; Dey, N. Cancer-Associated Fibroblast Functions as a Road-Block in Cancer Therapy. *Cancers* **2021**, *13*, 5246.
(5) Cirri, P.; Chiarugi, P. Cancer-associated-fibroblasts and tumour cells: a diabolic liaison driving cancer progression. *Cancer Metastasis Rev.* **2012**, *31*, 195−208.
(6) Garin-Chesa, P.; Old, L. J.; Rettig, W. J. Cell surface glycoprotein of reactive stromal fibroblasts as a potential antibody target in human epithelial cancers. *Proc. Natl. Acad. Sci. U.S.A.* **1990**, *87*, 7235−7239.
(7) Hessmann, E.; Buchholz, S. M.; Demir, I. E.; Singh, S. K.; Gress, T. M.; Ellenrieder, V.; Neesse, A. Microenvironmental Determinants of Pancreatic Cancer. *Physiol. Rev.* **2020**, *100*, 1707−1751.
(8) Hingorani, S. R. Epithelial and stromal co-evolution and complicity in pancreatic cancer. *Nat. Rev. Cancer* **2023**, *23*, 57−77.
(9) Norton, J.; Foster, D.; Chinta, M.; Titan, A.; Longaker, M. Pancreatic Cancer Associated Fibroblasts (CAF): Under-Explored Target for Pancreatic Cancer Treatment. *Cancers* **2020**, *12*, 1347.
(10) Jansen, K.; De Winter, H.; Heirbaut, L.; Cheng, J. D.; Joossens, J.; Lambeir, A. M.; De Meester, I.; Augustyns, K.; Van Der Veken, P. Selective inhibitors of fibroblast activation protein (FAP) with a xanthine scaffold. *Medchemcomm* **2014**, *5*, 1700−1707.
(11) Lindner, T.; Loktev, A.; Altmann, A.; Giesel, F.; Kratochwil, C.; Debus, J.; Jäger, D.; Mier, W.; Haberkorn, U. Development of Quinoline-Based Theranostic Ligands for the Targeting of Fibroblast Activation Protein. *J. Nucl. Med.* **2018**, *59*, 1415−1422.
(12) Zhao, L.; Chen, J.; Pang, Y.; Fu, K.; Shang, Q.; Wu, H.; Sun, L.; Lin, Q.; Chen, H. Fibroblast activation protein-based theranostics in cancer research: A state-of-the-art review. *Theranostics* **2022**, *12*, 1557−1569.
(13) Ding, J.; Qiu, J.; Hao, Z.; Huang, H.; Liu, Q.; Liu, W.; Ren, C.; Hacker, M.; Zhang, T.; Wu, W.; Li, X.; Huo, L. Comparing the clinical value of baseline [68 Ga]Ga-FAPI-04 PET/CT and [18F]F-FDG PET/CT in pancreatic ductal adenocarcinoma: additional prognostic value of the distal pancreatitis. *Eur. J. Nucl. Med. Mol. Imaging* **2023**, *50*, 4036−4050.
(14) Rohrich, M.; Naumann, P.; Giesel, F. L.; Choyke, P. L.; Staudinger, F.; Wefers, A.; Liew, D. P.; Kratochwil, C.; Rathke, H.; Liermann, J.; Herfarth, K.; Jager, D.; Debus, J.; Haberkorn, U.; Lang, M.; Koerber, S. A. Impact of 68Ga-FAPI PET/CT Imaging on the Therapeutic Management of Primary and Recurrent Pancreatic Ductal Adenocarcinomas. *J. Nucl. Med.* **2021**, *62*, 779−786.
(15) van der Heide, C. D.; Ma, H.; Hoorens, M. W. H.; Campeiro, J. D.; Stuurman, D. C.; de Ridder, C. M. A.; Seimbille, Y.; Dalm, S. U. In vitro and in vivo analyses of eFAP: a novel FAP-targeting small molecule for radionuclide theranostics and other oncological interventions. *EJNMMI Radiopharm. Chem.* **2024**, *9*, 55.
(16) van Dam, M. A.; Vuijk, F. A.; Stibbe, J. A.; Houvast, R. D.; Luelmo, S. A. C.; Crobach, S.; Shahbazi Feshtali, S.; de Geus-Oei, L. F.; Bonsing, B. A.; Sier, C. F. M.; Kuppen, P. J. K.; Swijnenburg, R. J.; Windhorst, A. D.; Burggraaf, J.; Vahrmeijer, A. L.; Mieog, J. S. D. Overview and Future Perspectives on Tumor-Targeted Positron Emission Tomography and Fluorescence Imaging of Pancreatic Cancer in the Era of Neoadjuvant Therapy. *Cancers* **2021**, *13*, 6088.
(17) Xu, M.; Zhang, T.; Xia, R.; Wei, Y.; Wei, X. Targeting the tumor stroma for cancer therapy. *Mol. Cancer* **2022**, *21*, 208.
(18) Saúde-Conde, R.; Arçay Öztürk, A.; Stosic, K.; Azurmendi Senar, O.; Navez, J.; Bouchart, C.; Arsenijevic, T.; Flamen, P.; Van Laethem, J. L. Cancer-Associated Fibroblasts in Pancreatic Ductal Adenocarcinoma or a Metaphor for Heterogeneity: From Single-Cell Analysis to Whole-Body Imaging. *Biomedicines* **2024**, *12*, 591.
(19) Houvast, R. D.; Badr, N.; March, T.; de Muynck, L. D. A. N.; Sier, V. Q.; Schomann, T.; Bhairosingh, S.; Baart, V. M.; Peeters, J. A. H. M.; van Westen, G. J. P.; Plückthun, A.; Burggraaf, J.; Kuppen, P. J. K.; Vahrmeijer, A. L.; Sier, C. F. M. Preclinical evaluation of EpCAM-binding designed ankyrin repeat proteins (DARPins) as targeting moieties for bimodal near-infrared fluorescence and photoacoustic imaging of cancer. *Eur. J. Nucl. Med. Mol. Imaging* **2024**, *51*, 2179−2191.
(20) Houvast, R. D.; Baart, V. M.; Bhairosingh, S. S.; Cordfunke, R. A.; Chua, J. X.; Vankemmelbeke, M.; Parsons, T.; Kuppen, P. J. K.; Durrant, L. G.; Vahrmeijer, A. L.; Sier, C. F. M. Glycan-based near-infrared fluorescent (NIRF) imaging of gastrointestinal tumors: a preclinical proof-of-concept in vivo study. *Mol. Imaging Biol.* **2020**, *22*, 1511−1522.
(21) Baart, V. M.; van der Horst, G.; Deken, M. M.; Bhairosingh, S. S.; Schomann, T.; Sier, V. Q.; van der Mark, M. H.; Iamele, L.; de Jonge, H.; Resnati, M.; Mazar, A. P.; Pelger, R. C. M.; van der Pluijm, G.; Kuppen, P. J. K.; Vahrmeijer, A. L.; Sier, C. F. M. A multimodal molecular imaging approach targeting urokinase plasminogen activator receptor for the diagnosis, resection and surveillance of urothelial cell carcinoma. *Eur. J. Cancer* **2021**, *146*, 11−20.
(22) de Valk, K. S.; Deken, M. M.; Handgraaf, H. J. M.; Bhairosingh, S. S.; Bijlstra, O. D.; van Esdonk, M. J.; Terwisscha van Scheltinga, A. G. T.; Valentijn, A. R. P. M.; March, T. L.; Vuijk, J.; Peeters, K. C. M. J.; Holman, F. A.; Hilling, D. E.; Mieog, J. S. D.; Frangioni, J. V.; Burggraaf, J.; Vahrmeijer, A. L. First-in-human assessment of cRGD-ZW800−1, a zwitterionic, integrin-targeted, near-infrared fluorescent peptide in colon carcinoma. *Clin. Cancer Res.* **2020**, *26*, 3990−3998.
(23) de Valk, K. S.; Deken, M. M.; Schaap, D. P.; Meijer, R. P.; Boogerd, L. S.; Hoogstins, C. E.; van der Valk, M. J.; Kamerling, I. M.; Bhairosingh, S. S.; Framery, B.; Hilling, D. E.; Peeters, K. C.; Holman, F. A.; Kusters, M.; Rutten, H. J.; Cailler, F.; Burggraaf, J.; Vahrmeijer, A. L. Dose-finding study of a CEA-targeting agent, SGM-101, for intra-operative fluorescence imaging of colorectal cancer. *Oncol* **2021**, *28*, 1832−1844.
(24) Stone, L. D.; Kasten, B. B.; Rao, S.; Gonzalez, M. L.; Stevens, T. M.; Lin, D.; Carroll, W.; Greene, B.; Moore, L. S.; Fuson, A.; James, S.; Hartman, Y. E.; McCammon, S.; Panuganti, B.; Nabell, L. M.; Li, Y.; Li, M.; Bailey, L.; Rosenthal, E. L.; Jeyarajan, H.; Thomas, C. M.; Warram, J. M. Interim Phase II Results Using Panitumumab-IRDye800CW during Transoral Robotic Surgery in Patients with Oropharyngeal Cancer. *Clin. Cancer Res.* **2024**, *30*, 4016−4028.

https://doi.org/10.1021/acs.bioconjchem.5c00218
Bioconjugate Chem. 2025, 36, 2145−2157

(25) Beffa, E. D.; Lyberis, P.; Rosboch, G. L.; Arezzo, A.; Lococo, F.; Carena, L.; Sciorsci, E.; Monica, V.; Lausi, P. O.; Dusi, V.; Busardò, F. P.; Buffa, E.; Stefania, R.; Ciccone, G.; Monagheddu, C.; Capello, B. M.; Vancheri, R.; Garrone, P.; Gabbarini, F.; Cattel, F.; Ruffini, E.; Guerrera, F. Study protocol for Near-infrared molecular imaging for lung cancer detection and treatment during mini-invasive surgery (phase II Trial) - (the RECOGNISE study). *BMC Cancer* **2024**, *24*, 1078.
(26) Hamdy, F. C.; Lamb, A. D.; Tullis, I. D. C.; Verrill, C.; Rombach, I.; Rao, S. R.; Colling, R.; Barber, P. R.; Volpi, D.; Barbera-Martin, L.; Lopez, J. F.; Omer, A.; Hewitt, A.; Lovell, S.; Niederer, J.; Lambert, A.; Snoeck, J.; Thomson, C.; Leslie, T.; Bryant, R. J.; Mascioni, A.; Jia, F.; Torgov, M.; Wilson, I.; Gudas, J.; Wu, A. M.; Olafsen, T.; Vojnovic, B. First-in-man study of the PSMA Minibody IR800-IAB2M for molecularly targeted intraoperative fluorescence guidance during radical prostatectomy. *Eur. J. Nucl. Med. Mol. Imaging* **2024**, *51*, 3009−3025.
(27) Vuijk, F. A.; de Muynck, L. D. A. N.; Franken, L. C.; Busch, O. R.; Wilmink, J. W.; Besselink, M. G.; Bonsing, B. A.; Bhairosingh, S. S.; Kuppen, P. J. K.; Mieog, J. S. D.; Sier, C. F. M.; Vahrmeijer, A. L.; Verheij, J.; Fariña-Sarasqueta, A.; Swijnenburg, R. J. Molecular targets for diagnostic and intraoperative imaging of pancreatic ductal adenocarcinoma after neoadjuvant FOLFIRINOX treatment. *Sci. Rep.* **2020**, *10*, 16211.
(28) Awad, S.; Alkashash, A. M.; Amin, M.; Baker, S. J.; Rose, J. B. Biochemical Predictors of Response to Neoadjuvant Therapy in Pancreatic Ductal Adenocarcinoma. *Front. Oncol.* **2020**, *10*, 620.
(29) Versteijne, E.; Van Dam, J. L.; Suker, M.; Janssen, Q. P.; Groothuis, K.; Akkermans-Vogelaar, J. M.; Besselink, M. G.; Bonsing, B. A.; Buijsen, J.; Busch, O. R.; Creemers, G. J. M.; Van Dam, R. M.; Eskens, F. A. L. M.; Festen, S.; De Groot, J. W. B.; Groot Koerkamp, B.; De Hingh, I. H.; Homs, M. Y. V.; Van Hooft, J. E.; Kerver, E. D.; Luelmo, S. A. C.; Neelis, K. J.; Nuyttens, J.; Paardekooper, G. M. R. M.; Patijn, G. A.; Van Der Sangen, M. J. C.; De Vos-Geelen, J.; Wilmink, J. W.; Zwinderman, A. H.; Punt, C. J.; Van Tienhoven, G.; Van Eijck, C. H. J. Neoadjuvant Chemoradiotherapy Versus Upfront Surgery for Resectable and Borderline Resectable Pancreatic Cancer: Long-Term Results of the Dutch Randomized PREOPANC Trial. *J. Clin. Oncol.* **2022**, *40*, 1220−1230.
(30) Slania, S. L.; Das, D.; Lisok, A.; Du, Y.; Jiang, Z.; Mease, R. C.; Rowe, S. P.; Nimmagadda, S.; Yang, X.; Pomper, M. G. Imaging of Fibroblast Activation Protein in Cancer Xenografts Using Novel (4-Quinolinoyl)-glycyl-2-cyanopyrrolidine-Based Small Molecules HHS Public Access. *J. Med. Chem.* **2021**, *64*, 4059−4070.
(31) Harryvan, T. J.; Hawinkels, L. J. A. C.; Inderson, A.; van Hooft, J. E.; Micke, P.; Johansen, J. S.; van Wezel, T.; Crobach, S.; Baart, V. M.; Quist, B. S.; Roet, J. E. G.; Kop, M. E.; Östman, A.; ten Dijke, P.; Strell, C.; Hornsveld, M. A Novel Pancreatic Cancer Mini-tumor Model to Study Desmoplasia and Myofibroblastic Cancer-Associated Fibroblast Differentiation. *Gastro Hep Adv.* **2022**, *1*, 678−681.

https://doi.org/10.1021/acs.bioconjchem.5c00218
Bioconjugate Chem. 2025, 36, 2145−2157